The Journal of Green Energy and Environmental Engineering

Review Paper

Research Progress and Prospects of Phosphorus-Based New Energy Battery Materials

Elizabeth Lich[1], Gathaniel G. Osgood[2,*]

[1] Department of Mathematics and Science Education, Middle East Technical University, Ankara, Turkey
[2] Biotechnology Laboratory, Study Center for Research and Biological Evaluations, Institute of Pharmacy and Foods, Havana University, Havana, Cuba
*Corresponding author:elich@agri.edu.tr; ggo00@ifal.euh.cu

Abstract. Amid escalating worldwide energy requirements and intensifying environmental imperatives, the advancement of novel energy materials has surfaced as a central research priority. The phosphorus chemical sector, constituting an integral component of the emerging energy landscape, fulfills a critical function in catalyzing green energy industry proliferation. This discourse examines the deployment of phosphate-derived materials within next-generation battery technologies, encompassing cathode compositions such as lithium iron phosphate and lithium manganese iron phosphate for lithium-ion systems, alongside sodium vanadium phosphate with NASICON framework architecture for sodium-ion battery negative electrodes. The research progress in liquid lithium salt electrolyte $LiPF_6$, solid electrolyte superionic conductor lithium aluminum titanium-phosphate and anode electrode materials such as phosphorus and phosphorus compounds were discussed. The characteristics of these materials and the possible challenges in the process of implementation were presented, such as the poor electrochemical stability of phosphorous cathode materials due to low electrical conductivity, which could be improved by material modification and nano-chemical synthesis technology. The research and application of phosphate-based new energy materials would continue to promote the growth of green energy industry and provide new ideas and solutions to solve energy and environmental problems..

Keywords: *phosphorus chemical industry; phosphorus-containing materials; NASICON structure; solid-state electrolytes; phosphorus-based anodes*

Received on 15 Feb 2026, Accepted on 15 May 2026, Published on 22 July 2026

1 Introduction

With the continuous transformation of diversified global energy structures and the rising advocacy of sustainable development concepts, the research and development of new energy materials have become a frontier in the industry. Lithium-ion batteries, distinguished by their superior energy density, cycling stability, and minimal self-discharge characteristics, have emerged as critical energy storage solutions for portable electronics, electric vehicles, and grid-scale storage applications [1]. Battery performance is predominantly governed by constituent active materials, encompassing cathode formulations [including lithium cobalt oxide, lithium iron phosphate, and nickel-cobalt-manganese layered oxides] and anode materials [such as graphite and silicon-based systems], which currently represent focal points of intensive research [2-4].

Phosphorus-based materials have shown great potential in the field of new energy materials due to their advantages such as abundant resources, low toxicity and environmental friendliness. The pronounced electronegativity and substantial atomic dimensions of these materials confer exceptional electronic characteristics, rendering them suitable candidates for lithium-ion battery negative electrodes. Their theoretical lithium storage capacity exceeds that of graphite, thereby facilitating enhanced battery energy density. For example, in sodium-ion battery anode materials, phosphorus-based materials such as NiP_3 [5], CoP [6], FeP [7] and FeP_4 [8] have also shown the potential to improve battery performance due to their high theoretical capacity and suitable sodium ion embedding potential. In the lithium battery system, the reaction

mechanism between phosphorus and lithium promotes the improvement of energy conversion efficiency. Through doping, structural optimization and other methods, the conductivity of phosphorus-based materials is enhanced, and the charge-discharge performance and cycle stability of batteries are gradually improved.

In addition, although phosphorus-based materials face challenges such as volume expansion and structural instability during cycling, strategies such as nano-sizing, carbon coating and porous structure construction can significantly improve their cycle stability [9]. Various modifications not only reveal new compounds in phosphorus-based materials and their unique composition structures, but also provide new ways for the development of new energy materials. To a certain extent, compounds formed by phosphorus with elements such as sulfur and nitrogen provide innovative ideas for optimizing material performance [10].

This paper intends to comprehensively introduce the latest research progress and technological innovations of phosphorus-based materials in the field of battery technology, and prospectively look forward to the potential applications of phosphorus-based materials in future new energy technologies. These studies not only lay a solid theoretical foundation for the industrial application of phosphorus-based new energy materials, but also are of great significance for promoting the high-quality development of the phosphorus chemical industry. The classification of phosphorus-based battery materials is shown in Fig. 1.

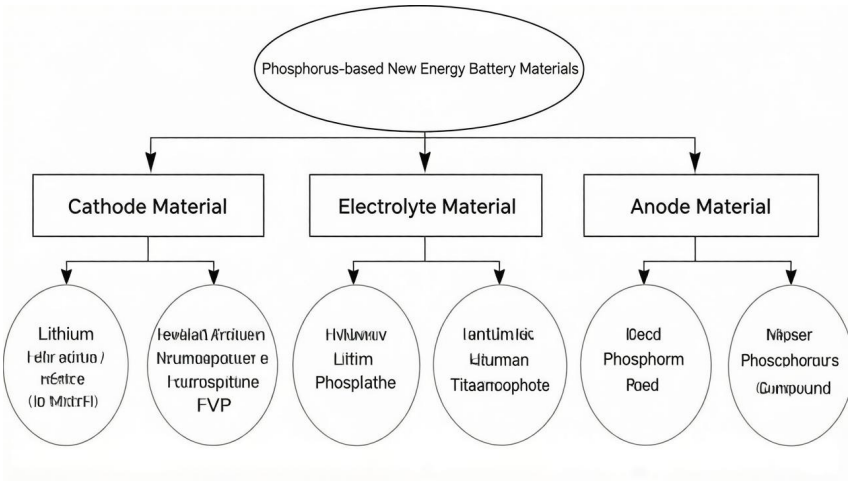

Figure 1 Classification of phosphorus-based new energy battery materials

2 Phosphorus-Based New Energy Battery Materials

2.1 Phosphorus-Based Cathode Materials

Phosphate-based cathode compositions constitute critical active materials within electrochemical energy storage architectures, including lithium-ion, sodium-ion, and zinc-ion battery systems. At present, a series of phosphate cathode materials have been developed, mainly including the following:

Lithium iron phosphate ($LiFePO_4$, LFP), a widely investigated cathode material for lithium-ion batteries, has garnered considerable research interest owing to its superior thermal stability and cycling durability. This compound crystallizes in the orthorhombic Pnma space group with an olivine-type structure, exhibiting lattice parameters of a = 1.0329 nm, b = 0.6011 nm, and c = 0.4699 nm. The crystal structure of this material is composed of FeO_6 and LiO_6 octahedra and PO_4 tetrahedra, as shown in Fig. 2.

Lithium manganese iron phosphate ($LiFe_{1-x}Mn_xPO_4$, LMFP), as a derivative of $LiFePO_4$, also shows good performance in lithium-ion batteries. Studies have shown that Fe doping replaces part of Mn, which not only improves the electrical conductivity of the material, but also effectively inhibits the Jahn-Teller effect of Mn^{3+}. This improvement endows LMFP with the high energy density of lithium manganese phosphate (LMP) and the excellent kinetic performance of LFP, making it an ideal substitute for LFP cathode materials. However, the

electrical conductivity of LMFP and the diffusion coefficient of Li^+ are relatively low, which limits its commercialization process to some extent [12]. Fig. 3 shows the crystal structure of LMFP.

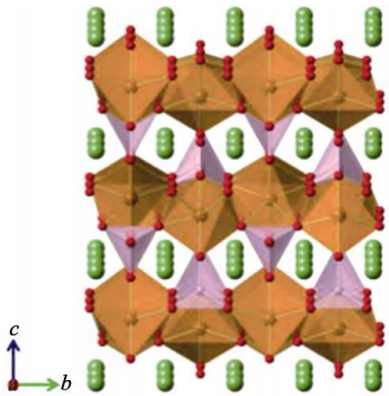

Figure 2 Olivine structure of $LiFePO_4$: FeO_6 octahedra (brown), PO_4 tetrahedra (purple) [11]

Sodium iron phosphate ($NaFePO_4$), a polyanion-type sodium-ion battery cathode material, has two crystal structures: olivine-type (t-$NaFePO_4$, t-NFP) and maricite-type (m-$NaFePO_4$, m-NFP), as shown in Fig. 4. In the t-$NaFePO_4$ structure, FeO_6 octahedra and PO_4 tetrahedra are connected by vertices to form a three-dimensional framework, providing a one-dimensional conduction channel for sodium ions along the b-axis, making it electrochemically active. In contrast, the FeO_6 octahedra and PO_4 tetrahedra in m-$NaFePO_4$ are arranged in a corner-sharing manner without forming sodium ion channels, so it is usually inactive. $NaFePO_4$ has application potential in the field of sodium-ion batteries due to its cost-effectiveness and abundant resources.

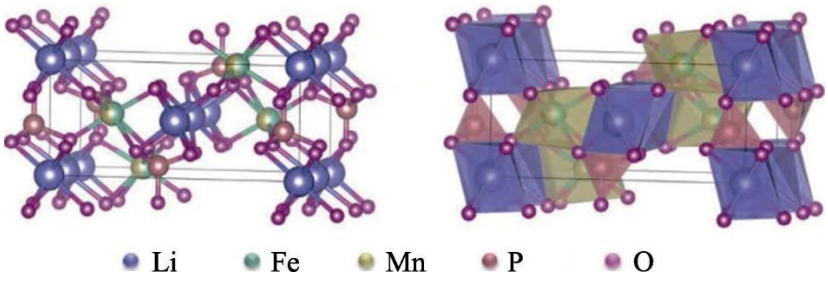

Figure 3 Crystal structure diagram of LMFP [13]

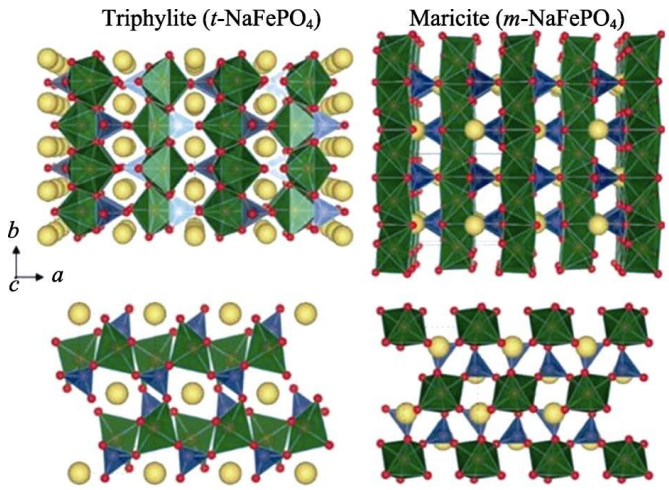

Figure 4 Schematic diagram of t-NFP (left) and m-NFP (right) polymorphs [FeO_6 octahedra (green), PO_4 tetrahedra (blue), and Na atoms (yellow)] [14]

Sodium superionic conductor (NASICON) structured $Na_3V_2(PO_4)_3$ and its derivatives $Na_3(VO)_2(PO_4)_2F$ and

transition metal fluorophosphates (A_2MPO_4F, where A = Li, Na; M = Mn, Fe, Co, Ni) constitute a class of phosphate-based materials, whose unique structural properties have opened up new paths for the advancement of battery technology.

NASICON-structured compounds occupy a place in the research and application of electrode materials and solid-state electrolytes due to their efficient sodium ion migration channels and robust three-dimensional frameworks. As shown in Fig. 5, the NASICON-type $Na_3V_2(PO_4)_3$ material is composed of a three-dimensional covalent framework [$V_2P_3O_{12}$], which is constructed from VO_6 octahedra and PO_4 tetrahedra, and contains Na1 and Na2 sodium ion tunnels.

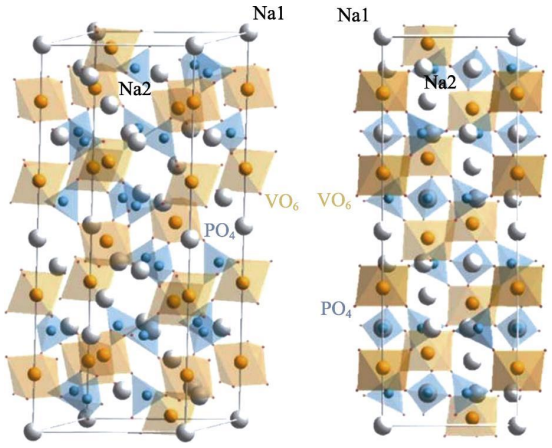

Figure 5 Crystal structure of $Na_3V_2(PO_4)_3$

In sodium-ion batteries, $Na_3V_2(PO_4)_3$ utilizes V^{3+}/V^{4+} and V^{2+}/V^{3+} redox couples to act as a cathode and anode at voltages of 3.4 V and 1.6 V, respectively, providing theoretical capacities of 118 mA·h/g and 50 mA·h/g. However, some $A_3M_2(PO_4)_3$-type compounds (where A = Li, Na; M = Cr, Fe, Zr) exhibit a monoclinic crystal system and undergo reversible structural phase transitions at high temperatures.

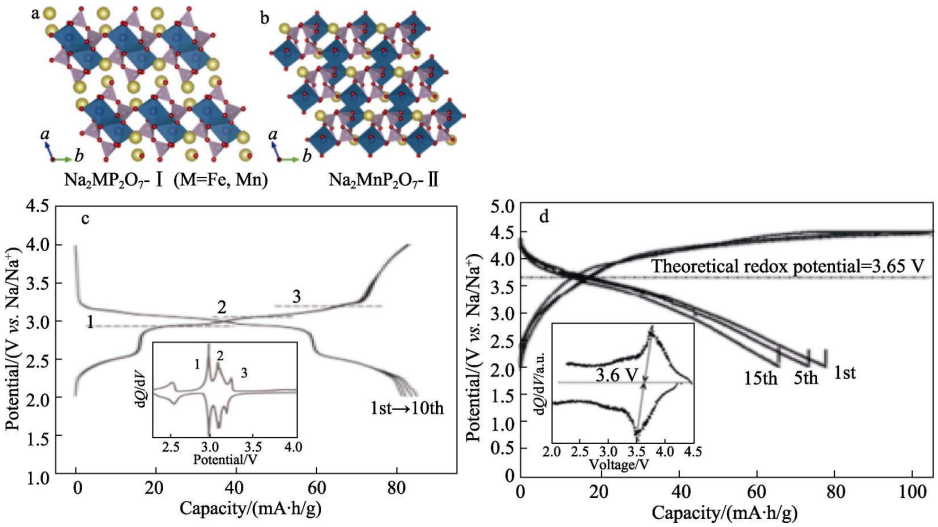

Figure 6 Crystal structure of $Na_2MP_2O_7$-I (M = Fe, Mn) (a) and $Na_2MnP_2O_7$-II [Fe/MnO_6 octahedra (green), PO_4 tetrahedra (purple) and Na atoms (yellow)] (b); Charge-discharge curves of $Na_2FeP_2O_7$ [15] (c) and $Na_2MnP_2O_7$ [16] (d)

Sodium pyrophosphate compositions ($Na_2MP_2O_7$, where M = Fe, Co, Mn, Cu) represent promising electrode materials for sodium-ion batteries, exhibiting favorable electrochemical characteristics. These compounds have diverse structures, such as triclinic, tetragonal and orthorhombic systems. Among them, $Na_2FeP_2O_7$ is a framework in which sodium atoms are embedded, constructed from FeO_6 octahedral dimers [Fe_2O_{11}] and PO_4

tetrahedra. BARPANDA et al. [15] applied it to sodium-ion batteries, and the material has a reversible capacity of 82 mA·h/g and a Fe^{2+}/Fe^{3+} redox potential of 2.5–3.0 V. In addition, sodium manganese pyrophosphate ($Na_2MnP_2O_7$) exhibits triclinic variants of $Na_2MnP_2O_7$-I and $Na_2MnP_2O_7$-II, which have similar structural frameworks but differ in unit cell dimensions and bond angles of Mn–O–Mn and P–O–P (Fig. 6a–c).

PARK et al. [16] investigated the application of $Na_2MnP_2O_7$ in sodium-ion battery systems, demonstrating that this material exhibits exceptional electrochemical performance at approximately 3.8 V (vs. Na^+/Na), delivering a reversible discharge capacity of up to 90 mA·h/g (Fig. 6d). The performance comparison of phosphate-based electrode materials applied in batteries and commercial lead-acid batteries is shown in Table 1.

Relative to conventional lead-acid battery technology, phosphate-based electrode material systems have garnered extensive research attention and practical deployment across diverse electrochemical storage platforms, attributable to their distinctive physicochemical attributes including elevated theoretical capacity, robust cycling stability, favorable thermal resilience, and ecological compatibility. Moving forward, sustained advancements in battery engineering will continue to propel performance enhancements in these materials, thereby driving progress in energy storage architectures and emerging power system technologies.

2.2 Phosphorus-Based Electrolyte Materials

Electrolytes serve as essential ion-transport media within battery systems, with their intrinsic properties exerting direct influence on operational efficiency, safety margins, and service longevity. Traditional electrolytes are composed of solvents, solutes and additives. Traditional solvents include polycarbonate (PC), diethyl carbonate (DEC) and ethyl methyl carbonate (EMC); while new solvents include carboxylate esters, nitrite esters and fluorinated solutions. Additives include functional additives such as film-forming, overcharge protection, high/low temperature and rate-type additives to improve the comprehensive performance of electrolytes. Lithium salt solutes are crucial to battery performance in electrolytes, mainly affecting ion transport efficiency, interface stability and inhibition of dendrite growth. The performance comparison of lithium salt electrolytes is shown in Table 2.

Table 1 Comparison of performance of phosphate-based electrode materials in batteries with commercial lead-acid batteries

Key indicator	Sodium-ion battery (Polyanion-type phosphorus-based cathode material)	Lithium-ion battery (Lithium (manganese) iron phosphate)	Lead-acid battery
Energy density/(Wh/kg)	100–120	140–170	30–50
Cycle life/cycles	7000–10000	>6000	500–1000
Low-temperature performance (-20°C)	90%	<70%	<60%
Rate performance	95% of 1C capacity at 5C discharge	90% of 1C capacity at 3C discharge	Poor
Tap density/(g/cm³)	2.1	2.2–2.5	—
Cathode material cost/(10^4 yuan/t)	2.5	3	1.6
Cell-level cost per kWh/[yuan/(W·h)]	0.31	0.45	0.4

Key indicator	Sodium-ion battery (Polyanion-type phosphorus-based cathode material)	Lithium-ion battery (Lithium (manganese) iron phosphate)	Lead-acid battery
Environmental friendliness	Excellent	Excellent	Poor

Note: "—" indicates no data available.

Table 2 Comparison of the performance of lithium salt electrolytes

Lithium salt type	Lithium hexafluorophosphate ($LiPF_6$)	Lithium bis(fluorosulfonyl)imide (LiFSI)	Lithium tetrafluoroborate ($LiBF_4$)	Lithium bis(oxalato)borate (LiBOB)	Lithium difluoro(oxalato) borate (LiODFB)
Ionic conductivity	Relatively high	High	Low	Relatively high	High
Melting point/°C	200	128	300	300	265
Solubility in water	Good	Poor	Good	Poor	Fair
Thermal stability	Poor	Good	Good	Good	Good
Advantages	Relatively high ionic conductivity; synergizes with carbonate solvents to form a stable solid electrolyte interphase (SEI) film on graphite surface, improving battery cycle performance; can form a stable passivation film on aluminum foil surface	High ionic conductivity, effectively improves low-temperature discharge performance and cycle life, good safety	Wide operating temperature range, good high/low temperature performance; can enhance electrolyte film-forming ability, inhibit current collector corrosion; has passivation protection for positive Al foil current collectors	Higher conductivity, wide operating temperature range; good cycle performance; insensitive to water	Good low-temperature performance, good cycle performance; forms a stable SEI film

Among many solute lithium salts, $LiPF_6$ is widely used due to its high ionic conductivity, good solubility, stable thermal performance, excellent battery cycle performance and environmental friendliness. However, $LiPF_6$ has relatively low thermal stability and is sensitive to moisture, which may limit its long-term stability in battery systems. To overcome these limitations, new lithium salts are being explored, such as ionic liquids or LiFSI, LiODFB, LiBOB combined with $LiPF_6$ to enhance its stability.

Solid-state electrolytes, functioning as rapid ionic conductors, hold substantial application potential across electrochemical energy storage, high-energy-density battery systems, and electromechanical devices owing to their superior ionic transport properties coupled with suppressed electronic conductivity. They constitute the critical enabling component for all-solid-state lithium and sodium-ion battery architectures, enhancing operational safety and cycle longevity while effectively mitigating risks associated with overcharge-induced thermal runaway and spontaneous ignition. In 1976, GOODENOUGH et al. [18] and HONG [19] reported NASICON, one of the earliest ion conductors discovered and deeply studied. The general formula of NASICON

structure is $AM_2(PO_4)_3$, where A is an alkali metal ion (such as Li^+, Na^+, K^+), and M is a tetravalent ion (such as Ge^{4+}, Ti^{4+}, Zr^{4+}). It crystallizes in the R-3c space group, with its framework assembled from MO_6 octahedra and PO_4 tetrahedra interconnected through oxygen bridges to generate a three-dimensional network architecture. This material has high ion conduction capacity and good chemical and electrochemical stability, making it an excellent solid-state electrolyte material. Na^+ is located between octahedra and migrates under an electric field to realize ion conduction. Although replacing Na^+ with Li^+ can be applied to lithium-ion batteries, the migration efficiency of Li^+ in the NASICON structure is low due to the difference in ion radii [20]. Li^+ conductors using the NASICON structure are rare in solid-state electrolytes. LATP has the chemical formula $Li_{1.3}Al_{0.3}Ti_{1.7}(PO_4)_3$, and is an ideal choice for high-voltage cathode materials due to its excellent oxidation potential [21]. In addition, LATP exhibits the highest ionic conductivity (1×10^{-4}–1×10^{-3} S/cm) among solid-state electrolytes and the best air stability among all similar materials, making it a popular candidate in the field of solid-state batteries [22]. LATP has an R-3c space group. By partially replacing Ti^{4+} in $LiTi_2(PO_4)_3$ with Al^{3+}, extra Li^+ can be introduced to maintain charge balance, thereby increasing the concentration and conductivity of Li^+. The crystal structure of LATP is shown in Fig. 7.

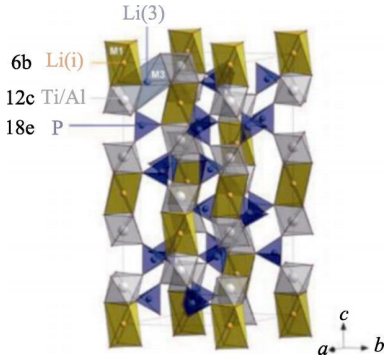

Figure 7 Crystal structure of LATP [23]

NASICON-type solid-state electrolyte lithium aluminum titanium phosphate has become a research hotspot due to its unique structure and performance. Nevertheless, its practical deployment in all-solid-state lithium battery configurations remains constrained by electrochemical stability limitations and elevated interfacial impedance. The key to addressing these challenges lies in improving the interface between LATP and the active part of electrode materials.

2.3 Phosphorus-Based Anode Materials

In recent years, significant progress has been made in the development of next-generation lithium-ion battery anode materials, which aim to achieve higher energy density and faster charge-discharge rates. Among the three allotropes of phosphorus, white phosphorus is usually not used as an electrode material due to its instability. Red phosphorus and black phosphorus have become hotspots in anode material research due to their better safety and stability [24]. Red phosphorus is a purplish-red amorphous powder, insoluble in water and common organic solvents, stable at room temperature, with a sublimation temperature of 416°C. Black phosphorus is a black crystal with the best conductivity and stability, with metallic luster. Its structures include orthorhombic, simple cubic, rhombic and amorphous forms. The honeycomb structure of orthorhombic black phosphorus is formed by phosphorus atoms connected via covalent bonds, with strong covalent bonds formed by Z-shaped chains between intra-layer atoms, and inter-layer attraction via van der Waals forces. The two-dimensional form of black phosphorus [25], namely black phosphorene, shows application potential in the energy storage field due to its large interlayer spacing [26].

As a promising anode material, phosphorus has attracted much attention due to its ability to improve electron transfer capacity for Li^+. During Li^+ intercalation, phosphorus can provide a theoretical specific capacity of up to 2595 mA·h/g [27], which is significantly higher than many traditional anode materials, indicating its broad prospects in high-rate and high-capacity battery applications. Phosphorus as an anode material faces problems including poor conductivity, large volume expansion and difficult synthesis, which can be improved by designing micro/nano structures, preparing composites of phosphorus with carbon or non-carbon materials,

and surface modification or doping.

3 Research Status of Phosphorus-Based New Energy Materials

Phosphorus-based materials mainly face two limiting factors in energy storage applications: one is low electronic conductivity, leading to actual charge-discharge specific capacity far lower than the theoretical value; the other is significant volume expansion during Li^+ intercalation/deintercalation, which negatively affects their electrochemical performance [28]. Nano-sizing technology and doping can improve the ion and electron transport properties of these materials, thereby reducing volume expansion and shortening transport paths [29].

3.1 Phosphorus-Based Cathode Materials

$LiFePO_4$, as a polyanion cathode material, is widely regarded as the best choice among lithium-ion battery cathode materials due to its stable discharge platform at 3.4 V, high discharge capacity of 170 mA·h/g, excellent cycle and thermal stability, cost-effectiveness, safety and environmental protection characteristics [30]. However, the discontinuous FeO_6 edge-sharing octahedral network in the $LiFePO_4$ crystal and the PO_4 tetrahedra between them affect electron transfer and Li^+ intercalation/deintercalation. In addition, the Li^+ diffusion path is easily blocked by Fe–Li antisite defects, resulting in a Li^+ diffusion coefficient far lower than the theoretical value [31]. The modification methods for $LiFePO_4$ materials include carbon coating process [32], ion doping process [33], and nano-sized particle regulation synthesis technology [34]. Carbon surface modification, characterized by economic viability and operational simplicity, currently represents the predominant approach for enhancing the electrochemical performance of lithium iron phosphate [35].

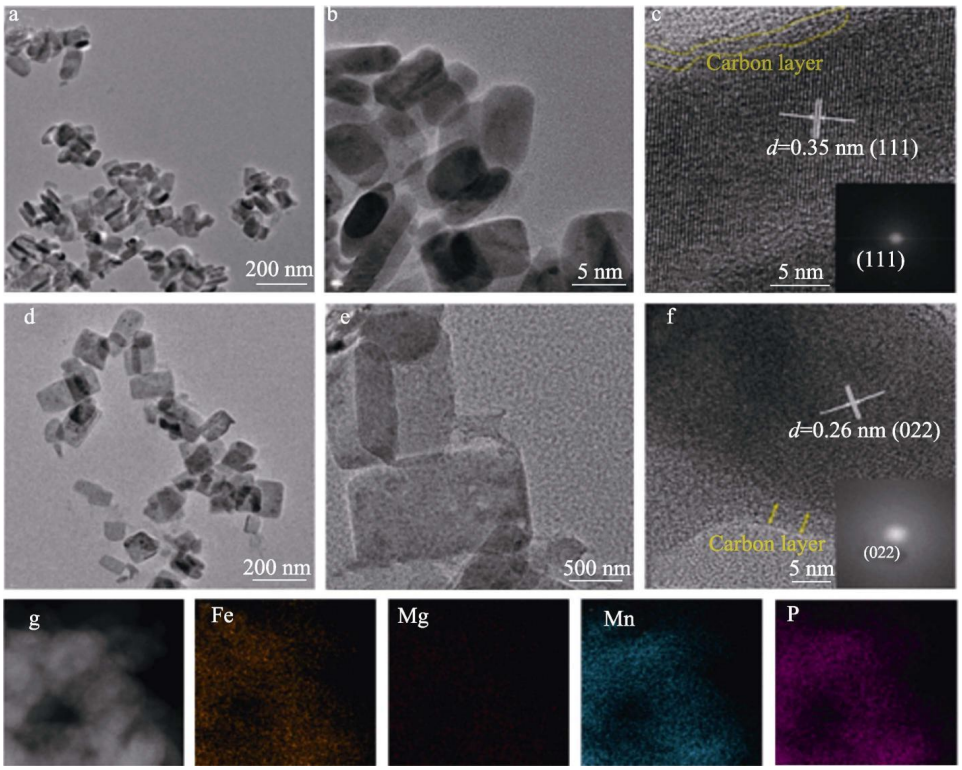

Figure 8 TEM and HRTEM images of LMFP-0 (a–c) and LMFP-2 (d–f); EDXS spectra of LMFP-2 (g)

LMFP deployment is constrained by the inherently limited electronic conductivity of the olivine-type $LiFePO_4$ framework. To enhance LMFP kinetic performance, HU et al. [36] synthesized magnesium-doped LMFP/C nanoplates through a facile, controllable solvothermal protocol. Investigations confirmed effective incorporation of Mg^{2+} into the crystalline lattice with partial substitution at Li^+ crystallographic sites. The optimized composition $Li_{0.97}Mg_{0.015}Mn_{0.8}Fe_{0.2}PO_4$ (designated LMFP-2) demonstrated exceptional

electrochemical characteristics with promising applicability in electric vehicle and grid-scale storage systems, delivering an elevated initial discharge capacity of 156.9 mA·h/g at 0.1C. Moreover, under aggressive rate conditions of 10C and 20C, LMFP-2 retained discharge capacities of 120.7 and 104.8 mA·h/g, with discharge processes completed within merely 255 and 110 seconds, respectively. These findings demonstrate that Li^+ site substitution with Mg^{2+} effectively enhances both electronic conductivity and lithium ion mobility within the material, thereby amplifying overall electrochemical performance. The rapid discharge capability and cycling stability of the synthesized material confer substantial application potential for high-performance lithium-ion battery systems. Comprehensive material characterization is presented in Fig. 8.

In addition, NASICON-type $Na_3V_2(PO_4)_3$ has attracted much attention due to the stability of its three-dimensional structure and high-voltage characteristics. However, its low electronic conductivity and limited redox couples restrict its energy density. CHEN et al. [37] replaced part of V^{3+} with Mn^{3+} to activate the V^{4+}/V^{5+} redox couple, significantly improving the energy density. Following dopant incorporation, the bandgap narrowed to 1.406 eV, electronic conductivity was enhanced, and four stable oxidation states were accessible for sequential redox conversion within the 1.4–4.0 V potential window, corresponding to a three-electron reversible reaction. Manganese-doped $Na_3V_2(PO_4)_3$ delivered a discharge specific capacity of 170.9 mA·h/g and energy density of 577 W·h/kg at 0.5C. YANG et al. [38] synthesized zinc-doped sodium vanadium manganese phosphate [$Na_4MnV(PO_4)_3$, NMVP] with a uniform carbonized polyacrylonitrile surface coating (NMZVP@cPAN) via the sol-gel methodology. The carbonized PAN layer was homogeneously distributed across the NMVP particle surface. This material exhibited exceptional rate capability (70.6 mA·h/g at 30C) and pronounced cycling stability (89.64% capacity retention after 1000 cycles at 5C). Crystallographic evolution was elucidated through Rietveld refinement and ex-situ X-ray diffraction analysis. The influence of zinc doping on electronic density of states and ion migration barriers was determined through density functional theory computations. The modified NMZVP@cPAN cathode was successfully implemented as an NMVP-type positive electrode material in sodium-ion battery configurations.

3.2 Phosphorus-Based Electrolyte/Solid-State Electrolyte Materials

As the core solute of lithium battery electrolytes, $LiPF_6$ has a significant impact on electrolyte cost. It is widely used in commercial lithium batteries due to its high ion mobility, moderate dissociation constant, excellent conductivity, electrochemical stability, good oxidation resistance and aluminum foil passivation effect. The industrial synthesis process of $LiPF_6$ mainly uses organic solvents and anhydrous HF as solvents. The comparison of the two mainstream processes is shown in Table 3.

Table 3 Two main production processes for $LiPF_6$

Production process	Organic solvent method	Anhydrous HF solvent method
Method	LiF and PF_5 are dissolved in organic solvents (such as carbonates, nitriles, ethers) for continuous reaction to generate $LiPF_6$.	LiF is dissolved in anhydrous HF to form a uniform LiF·HF solution, followed by feeding PF_5 gas to generate $LiPF_6$ via reaction.
Advantages	Mild operating conditions, high yield, low large-scale production cost; avoids corrosive substances compared with the HF solvent method, reducing equipment requirements.	Simple and controllable process, low impurity content after crystallization, high purity.
Disadvantages	PF_5 easily undergoes side reactions with solvents, making product impurity removal difficult; suitable for preparing liquid $LiPF_6$.	Due to the strong corrosiveness of HF, special requirements for equipment and pipelines, resulting in high equipment requirements, high energy consumption and high cost.

Production process	Organic solvent method	Anhydrous HF solvent method
Representative enterprises	Guangzhou Tinci Materials Technology Co., Ltd.	Do-fluoride New Materials Co., Ltd.

In the industrialization process, the $LiPF_6$ industry faces multiple challenges, including overcapacity, sensitivity to moisture, insufficient thermal stability, high production cost, equipment corrosion and environmental pollution. To address these challenges, synthetic efficiency and product purity can be improved via technological innovation; processes can be optimized and automation increased to reduce costs; environmental investment can be increased to reduce pollution. These measures will jointly promote the sustainable and healthy development of the $LiPF_6$ industry.

As a commonly used lithium salt, $LiPF_6$ shows insufficient moisture and thermal stability under high voltage and high temperature, making it difficult to meet the application requirements of lithium metal batteries (LMBs). CHEN et al. [39] showed that boron-doped lithium difluoro(oxalato)borate (LiFPB) effectively solves the stability problem of $LiPF_6$ under high voltage and high temperature environments. This compound exhibits exceptional thermal resilience and electrochemical stability, does not generate hydrogen fluoride upon decomposition, and can establish a protective surface film on $LiCoO_2$. Its anionic species facilitate formation of a rapid ion-conducting solid electrolyte interphase at the lithium metal anode, substantially enhancing battery cycling performance under extreme operational conditions. Empirical data demonstrate that LCO/Li cells employing LiFPB retain 80% capacity after 260 cycles at 60 °C and 4.45 V, with sustained favorable performance even at 100 °C. Fig. 9 is a schematic diagram of the mechanism and action of LiFPB compared with $LiPF_6$, where CEI refers to the cathode-electrolyte interphase layer.

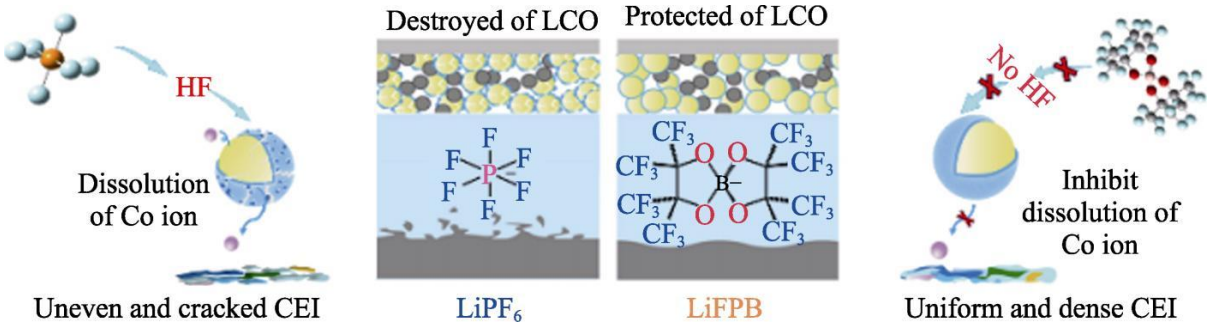

Figure 9 Schematic diagram of mechanism and action of LiFPB and $LiPF_6$

Solid lithium/sodium-ion batteries are regarded as strong candidates for next-generation energy storage systems due to their high energy density and safety. However, interface resistance and dendrite problems, especially under high current densities, limit their development. Lithium aluminum titanium phosphate solid-state electrolyte offers numerous advantages including elevated ionic conductivity, favorable atmospheric stability, and low feedstock costs, presenting substantial industrial development potential. Nevertheless, existing fabrication protocols remain inadequate for large-scale manufacturing requirements. HE et al. [40] introduced a streamlined solid-liquid hybrid synthesis route for LATP preparation. Through reactant optimization and implementation of a vacuum self-mixing protocol, high-purity, high-performance LATP solid-state electrolyte was achieved even in the absence of conventional mechanical mixing. The material exhibited total ionic conductivity of 1.7 mS/cm at ambient temperature, with bulk conductivity reaching 7.2 mS/cm—both representing record values in published literature. The as-obtained pellet demonstrated exceptional densification at 99.4% theoretical density. This methodology additionally circumvents challenges associated with material adhesion to processing vessels and diminished sintering yields characteristic of traditional thermal consolidation approaches, furnishing a more accessible technical pathway for LATP solid-state electrolyte commercialization. The fabrication sequence is schematically illustrated in Fig. 10.

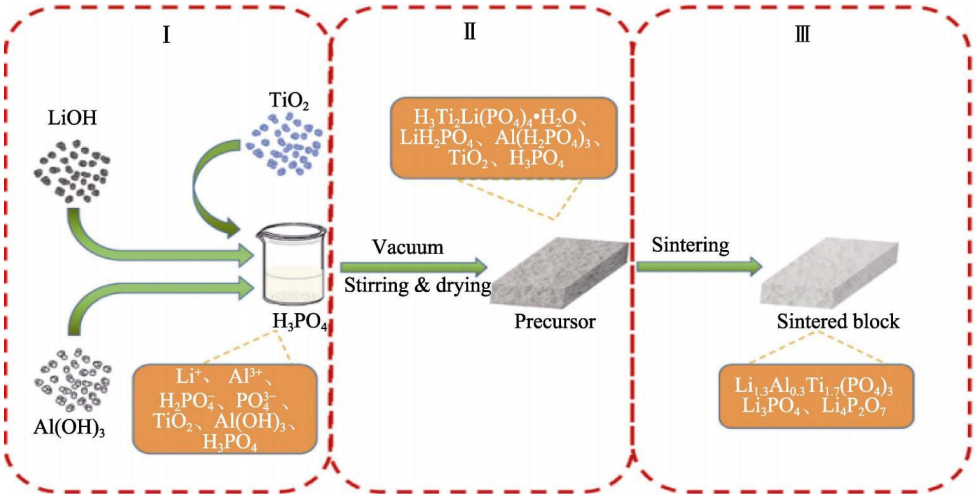

Figure 10 Schematic diagram of preparation process of LATP solid-state electrolyte

3.3 Phosphorus-Based Anode Materials

Investigation into orthorhombic black phosphorus as a lithium storage medium was initiated in 2007. PARK et al. [41] demonstrated that this allotrope delivers an exceptionally high initial discharge specific capacity exceeding 2100 mA·h/g at 100 mA/g current density; however, the first-cycle Coulombic efficiency was merely 57%, with capacity rapidly deteriorating to 220 mA·h/g within 30 cycles. This pronounced capacity fade was primarily attributed to substantial volumetric expansion and consequent mechanical pulverization during lithium insertion. In 2012, SUN et al. [42] prepared black phosphorus via the high-temperature and high-pressure method, and the initial discharge specific capacity reached 2649 mA·h/g under optimized conditions, but the specific capacity decreased to 703 mA·h/g after 60 cycles.

Combining nano-sized phosphorus materials with conductive carbon materials enhances their anode performance. The composite uses the conductivity of carbon to improve the electron conduction of phosphorus, and adopts a nanostructure to mitigate volume expansion, thereby improving its electrochemical lithium storage efficiency. For instance, YU et al. [43] fabricated a red phosphorus-graphene composite through ball milling, achieving nanoscale dimension reduction of red phosphorus and its uniform distribution within the graphene framework, thereby substantially enhancing electrochemical performance. This material delivered an initial discharge specific capacity of 2100 mA·h/g at 130 mA/g, with 61% capacity retention after 300 cycles and 73% capacity maintained following 200 cycles under elevated temperature conditions. YUAN et al. [44] further advanced specific capacity and cycling stability through process optimization involving pre-ball milling of red phosphorus followed by integration with carbon nanotubes. The initial charge specific capacity exceeded 2100 mA·h/g, with approximately 1000 mA·h/g retained after 50 cycles, validating the efficacy of nanoscale engineering and carbonaceous matrix compositing for red phosphorus electrochemical enhancement. Collectively, these investigations demonstrate that particle size reduction and hybridization with carbon materials effectively improve red phosphorus electrochemical characteristics, encompassing elevated specific capacity and enhanced cycle durability.

In addition, XIAO et al. [45] developed a 3D network binary polymer binder based on carboxymethyl cellulose (CMC) and polyethylene oxide (PEO) for black phosphorus-graphite (BP-G) composite anodes. The binder strengthens the cross-linking of CMC and PEO via intermolecular forces, and forms a stable combination with BP. Meanwhile, phosphorus-carbon (PC) bonds and phosphorus-oxygen-carbon (POC) bonds between BP and graphite enhance the overall structure of the composite. This structural design effectively alleviates the volume expansion problem of BP and maintains electrical contact between electrode components, thereby improving the electrochemical performance of the battery, achieving a high initial discharge specific capacity of 1602 mA·h/g at a current density of 0.5 A/g. Fig. 11 shows the formation process of black phosphorus cross-linked with two binders (CMC and PEO).

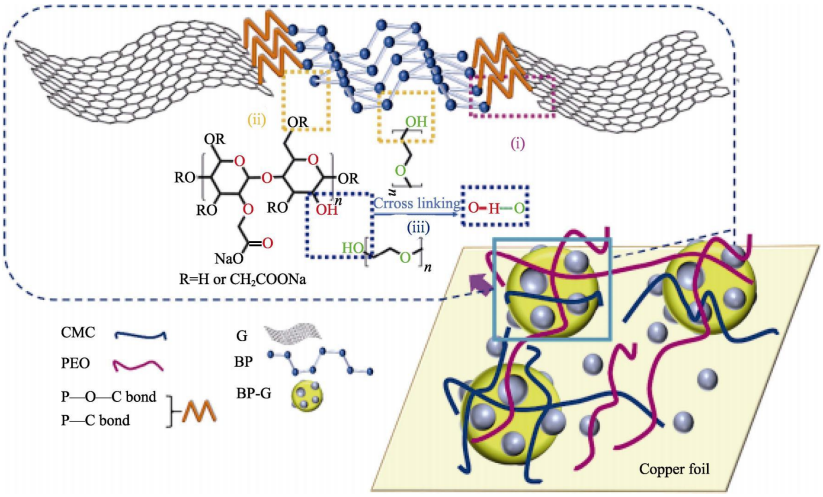

Figure 11 Schematic diagram of black phosphorus crosslinked with two binders (CMC and PEO)

4 Conclusion and Prospects

Amid the ongoing transformation of worldwide energy architectures and the accelerated proliferation of the new energy vehicle sector, investigations and practical deployment of phosphorus-derived energy materials have garnered escalating research interest. As a major phosphorus resource country, China has unique advantages in this field. At present, a variety of phosphorus-based materials in China have entered the industrialization stage, among which the most prominent is $LiFePO_4$ cathode material, which has been widely used in the power battery field due to its advantages such as long cycle life, high safety and low cost. In addition, China has also made significant progress in new energy materials such as phosphoric acid and $LiPF_6$, and achieved large-scale production. However, compared with the international advanced level, China still has problems such as insufficient depth of research and lack of technological breakthroughs in mastering core patents, producing high-purity fine phosphates, and improving the comprehensive utilization efficiency of resources, including energy consumption, environmental pollution, technical complexity and the effectiveness of resource utilization, all of which lag behind foreign countries. Weak innovation capabilities, environmental pressure and the need to improve the comprehensive utilization rate of phosphate mines have become important links hindering current development.

To accurately grasp the current development status, future work needs to focus on the following aspects: First, promote the industry to develop in a green and environmentally friendly direction, focus on the transformation to high-end refined product industries, and tap the potential of fine phosphorus chemicals and functional materials to realize the maximum added value benefit of products. Second, invest a large number of researchers and technologies to achieve breakthroughs in key technologies such as wet-process phosphoric acid refining and high-polymerization-degree ammonium polyphosphate, and concentrate comprehensive capabilities to improve product purity and quality, so as to grasp the forefront of development in the coming period. For the graded utilization of phosphate rock resources, in addition to graded processing of products, it is also necessary to optimize the resources of each part to maximize the utilization of medium- and low-grade phosphate rocks. For the recovery and utilization of associated resources, certain technologies should be used for recovery and treatment to better recycle resources and realize the effective and full utilization of resources. Third, pay attention to the research results of various scientific research institutions, and carry out cooperation and exchanges as much as possible under the premise of meeting development needs, so as to broaden industrial channels, expand the industrial chain of business development, and realize the coupling and symbiosis of resources. In addition, resource reorganization and mergers and acquisitions among enterprises should always develop in the direction of high-precision and cutting-edge products, dare to abandon or innovate backward production capacity and technical methods, and be good at reintegrating resource technologies in the context of synchronous domestic and international development, using domestic preferential policies to explore cross-field cooperative symbiosis, so as to optimize technology and realize the

maximum benefit of resources, ensuring the sustainable development of enterprises. Finally, in the adjustment of product structure, priority should be given to current advantageous products, and funds and technology should always support the development of new efficient phosphate fertilizers and functional phosphates, continuously realizing the transformation of the industry to service-oriented manufacturing, and continuously improving the overall competitiveness of products and the sustainable development of the industry while adapting to market development.

Looking to the future, the research and development of phosphorus-based new energy materials will continue to focus on breakthroughs in improving material performance, reducing costs, and enhancing safety and environmental friendliness. With the continuous expansion of the new energy vehicle and energy storage markets, the demand for high-performance phosphorus-based materials will increase day by day. With the tremendous changes in technological development and the strengthening of environmental awareness, the green and intelligent production of phosphorus-based materials will become the core of future development.

References

[1] Chen X B, Lu L, Yu P Y, et al. Increasing solar absorption for photocatalysis with black hydrogenated titanium dioxide nanocrystals. Science, 2011, 331(6018): 746-750.

[2] Li N, Zhang W, Li G X, et al. Research progress on TiO_2 photocatalysts. Fine Chemicals, 2021, 38(11): 2181-2188, 2258.

[3] Fuentes K M, Venuti D, Betancourt P. Black titania with increased defective sites for phenol photodegradation under visible light. Reaction Kinetics, Mechanisms and Catalysis, 2020, 131(1): 423-435.

[4] Andronic L, Lelis M, Enesca A, et al. Photocatalytic activity of defective black-titanium oxide photocatalysts towards pesticide degradation under UV/Vis irradiation. Surfaces and Interfaces, 2022, 32: 102123.

[5] Khanam R, Taparia D, Momdal B, et al. Black titania: Effect of hydrogenation on structural and thermal stability of nanotitania. Applied Physics A, 2016, 122(2): 92.

[6] Thakur N, Thakur N, Kumar A, et al. A critical review on the recent trends of photocatalytic, antibacterial, antioxidant and nanohybrid applications of anatase and rutile TiO_2 nanoparticles. Science of the Total Environment, 2024, 914: 169815.

[7] Haidner S, Nawaz R, Anjum M, et al. Property-performance relationship of core-shell structured black TiO_2 photocatalyst for environmental remediation. Frontiers of Environmental Science & Engineering, 2023, 17(9): 111.

[8] Soria J, Sanz J, Torralvo M J, et al. The effect of the surface disordered layer on the photoreactivity of titania nanoparticles. Applied Catalysis B: Environmental, 2017, 210: 306-319.

[9] Li Z, Wang E G, Zhang Y Z, et al. Antibacterial ability of black titania in dark: Via oxygen vacancies mediated electron transfer. Nano Today, 2023, 50: 101826.

[10] Jiang W B, Loh H Y, Low B Q L, et al. Role of oxygen vacancy in metal oxides for photocatalytic CO_2 reduction. Applied Catalysis B: Environmental, 2023, 321: 122079.

[11] Deskins N A, Du J, Rao P. The structural and electronic properties of reduced amorphous titania. Physical Chemistry Chemical Physics, 2017, 19(28): 18671-18684.

[12] Liu X G, Bi Y P. Synergistic effect of Ti^{3+} doping and facet regulation over Ti^{3+}-doped TiO_2 nanosheets with enhanced photoreactivity. Catalysis Science & Technology, 2018, 8(15): 3876-3882.

[13] Abdullah S A, Sahdan M Z, Nafarizal N, et al. Influence of substrate annealing on inducing Ti^{3+} and oxygen vacancy in TiO_2 thin films deposited via RF magnetron sputtering. Applied Surface Science, 2018, 462: 575-582.

[14] Gao X T. Study on photocatalytic properties based on TiO_{2-x} and its composites [D]. Harbin: Harbin Normal University, 2022.

[15] He M, Ji J, Liu B Y, et al. Reduced TiO_2 with tunable oxygen vacancies for catalytic oxidation of formaldehyde at room temperature. Applied Surface Science, 2019, 473: 934-942.

[16] Chen J, Ding Z Y, Wang C, et al. Black anatase titania with ultrafast sodium-storage performances stimulated by oxygen vacancies. ACS Applied Materials & Interfaces, 2016, 8(14): 9142-9151.

[17] Shi D X, Zhang H H, Gao X, et al. Research progress on the preparation and catalytic application of core-shell nanocomposites. Fine Chemicals, 2023, 40(1): 33-43.

[18] Hu W Y, Zhou W, Zhang K F, et al. Facile strategy for controllable synthesis of stable mesoporous black TiO_2 hollow spheres with efficient solar-driven photocatalytic hydrogen evolution. Journal of Materials Chemistry A, 2016, 4(19): 7495-7502.

[19] Zhang K, Park J H. Surface localization of defects in black TiO_2: Enhancing photoactivity or reactivity. The Journal of Physical Chemistry Letters, 2017, 8(1): 199-207.

[20] Zhang S S, Zhang S Q, Peng B Y, et al. High performance hydrogenated TiO_2 nanorod arrays as a photoelectrochemical sensor for organic compounds under visible light. Electrochemistry Communications, 2014, 40: 24-27.

[21] Wang Z, Yang C Y, Lin T, et al. H-doped black titania with very high solar absorption and excellent photocatalysis enhanced by localized surface plasmon resonance. Advanced Functional Materials, 2013, 23(43): 5444-5450.

[22] Pylnev M, Chang W H, Wong M S. Shell of black titania prepared by sputtering TiO_2 target in H_2+Ar plasma. Applied Surface Science, 2018, 462: 285-290.

[23] Ariyanti D, Mills L, Dong J, et al. $NaBH_4$ modified TiO_2: Defect site enhancement related to its photocatalytic activity. Materials Chemistry and Physics, 2017, 199: 571-576.

[24] Chen S H, Xiao Y, Wang Y H, et al. A facile approach to prepare black TiO_2 with oxygen vacancy for enhancing photocatalytic activity. Nanomaterials, 2018, 8(4): 245.

[25] Zheng P, Tang J L, Zhou Z P, et al. Ultrafast synthesis of defective black TiO_2 via one-step NaN_3 deflagration for high-efficiency solar water evaporation. Surfaces and Interfaces, 2020, 22: 100901.

[26] Wang Z, Yang C Y, Lin T Q, et al. Visible-light photocatalytic, solar thermal and photoelectrochemical properties of aluminium-reduced black titania. Energy & Environmental Science, 2013, 6(10): 3007-3014.

[27] Lin L X, Huang J T, Li X F, et al. Effective surface disorder engineering of metal oxide nanocrystals for improved photocatalysis. Applied Catalysis B: Environmental, 2017, 203: 615-624.

[28] Azab N A, El-Sharkawy A A M, Omran Z A, et al. C_3N_4 interlayer formation while synthesizing black titania and their dye sensitized solar cell and conductivity performances. Solar Energy Materials and Solar Cells, 2021, 232: 111347.

[29] Qi W T, Wang N, Chen X Y, et al. Plasmon-assisted partially reduced TiO_2 nanotube arrays for photoelectrochemical water splitting. Materials Research Express, 2020, 6(12): 1250h9.

[30] Li Z B, Bian H D, Xiao X F, et al. Defective black TiO_2 nanotube arrays for enhanced photocatalytic and photoelectrochemical applications. ACS Applied Nano Materials, 2019, 2(11): 7372-7378.

[31] Liu X, Xu H, Grabstanowicz L R, et al. Ti^{3+} self-doped TiO_{2-x} anatase nanoparticles via oxidation of TiH_2 in H_2O_2. Catalysis Today, 2014, 225: 80-89.

[32] Reddy Y A K, Kang I K, Shin Y B, et al. Oxygen atmosphere annealing effect on the thermal stability of TiO_{2-x} based films for shutter-less infrared image sensors. Key Engineering Materials, 2018, 775: 272-277.

[33] Su Y, Zhang W, Chen S M, et al. Engineering black titanium dioxide by femtosecond laser filament. Applied Surface Science, 2020, 520: 146298.

[34] Jedsukontorn T, Ueno T, Saito N, et al. Facile preparation of defective black TiO_2 through the solution plasma process: Effect of parametric changes for plasma discharge on its structural and optical properties. Journal of Alloys and Compounds, 2017, 726: 567-577.

[35] Raes A, Ninakanti R, Van den B L, et al. Black titania by sonochemistry: A critical evaluation of existing methods. Ultrasonics Sonochemistry, 2023, 100: 106601.

[36] Zhang L N, Liu T L, Liu T F, et al. Improving photocatalytic performance of defective titania for carbon dioxide photoreduction by Cu cocatalyst with SCN^- ion modification. Chemical Engineering Journal, 2023, 463: 142358.

[37] Bi Q Y, Song E, Chen J C, et al. Nano gold coupled black titania composites with enhanced surface plasma properties for efficient photocatalytic alkyne reduction. Applied Catalysis B: Environmental, 2022, 309: 121222.

[38] Cong T Z, Zhang Y F, Huang H, et al. Ag nanoparticles synthesized on black-titanium dioxide by photocatalytic method as reusable substrates of surface-enhanced Raman spectroscopy. Chemosensors, 2022, 10(11): 441.

[39] Yuan C F, Shen Y L, Zhu C Y, et al. Ru single-atom decorated black TiO_2 nanosheets for efficient solar-driven hydrogen production. ACS Sustainable Chemistry & Engineering, 2022, 10(31): 10311-10317.

[40] Yuan X T, Wang X, Liu X Y, et al. Ti^{3+}-promoted high oxygen-reduction activity of Pd nanodots supported by black titania nanobelts. ACS Applied Materials & Interfaces, 2016, 8(41): 27654-27660.

[41] Yang C Y, Wang Z, Lin T Q, et al. Core-shell nanostructured "black" rutile titania as excellent catalyst for

hydrogen production enhanced by sulfur doping. Journal of the American Chemical Society, 2013, 135(47): 17831-17838.

[42] Rahman S, Nawaz R, Khan J, et al. Synthesis and characterization of carbon and carbon-nitrogen doped black TiO_2 nanomaterials and their application in sonophotocatalytic remediation of treated agro-industrial wastewater. Materials, 2021, 14(20): 6175.

[43] Shafiee A, Carrier A J, Nganou C, et al. Mechanistic insight into the enhanced photodegradation by black titanium dioxide nanofiber-graphene quantum dot composites. Applied Surface Science, 2023, 636: 157836.

[44] Cui H, Cao J Y, Zhao Y, et al. Construction of IO-B-TiO_2/In_2O_3 S-scheme heterojunction with photothermal effects and its highly efficient photocatalytic reduction of CO_2 under full-spectrum light. Chemical Engineering Journal, 2024, 479: 147618.

[45] Li Y F, Feng Y C, Bai H, et al. Enhanced visible-light photocatalytic performance of black TiO_2/SnO_2 nanoparticles. Journal of Alloys and Compounds, 2023, 960: 170672.

[46] Li Z Z, Li H Z, Wang S J, et al. Mesoporous black TiO_2/MoS_2/Cu_2S hierarchical tandem heterojunctions toward optimized photothermal-photocatalytic fuel production. Chemical Engineering Journal, 2022, 427: 131830.

[47] Tan B Y, Ye X Z, Li Y J, et al. Defective anatase TiO_{2-x} mesocrystal growth in situ on g-C_3N_4 nanosheets: Construction of 3D/2D Z-scheme heterostructures for highly efficient visible-light photocatalysis. Chemistry—A European Journal, 2018, 24(50): 13311-13321.

[48] Li J, Jiang Z X, Li J F, et al. Synthesis of black titanium dioxide/activated carbon composites for enhanced visible-light photocatalytic properties. Journal of Materials Science: Materials in Electronics, 2024, 35(16): 1050.

[49] Zakaria H, Li Y, Fathy M M, et al. A novel TiO_{2-x}/TiN@ACB composite for synchronous photocatalytic Cr(VI) reduction and water photothermal evaporation under visible/infrared light illumination. Chemosphere, 2023, 311: 137137.

[50] Hu P W, Zhang Y, Cheng G L. Natural kaolinite modified black titanium dioxide for efficient visible light assisted photocatalysis. Molecular Catalysis, 2023, 547: 113312.

[51] Zhai M J, Liu Y, Huang J, et al. Efficient suspension plasma spray fabrication of black titanium dioxide coatings with visible light absorption performances. Ceramics International, 2019, 45(1): 930-935.

[52] Chen S H, Wang Y H, Li J, et al. Synthesis of black TiO_2 with efficient visible-light photocatalytic activity by ultraviolet light irradiation and low temperature annealing. Materials Research Bulletin, 2018, 98: 280-287.

[53] Saensook S, Sirisuk A. A factorial experimental design approach to obtain defect-rich black TiO_2 for photocatalytic dye degradation. Journal of Water Process Engineering, 2022, 45: 102495.

[54] Yuan X J, Sun M X, Yao Y, et al. N/Ti^{3+}-codoped triphasic TiO_2/g-C_3N_4 heterojunctions as visible-light photocatalysts for the degradation of organic contaminants. New Journal of Chemistry, 2019, 43(6): 2665-2675.

[55] Chen P. A novel synthesis of Ti^{3+} self-doped Ag_2O/TiO_2 (p-n) nanoheterojunctions for enhanced visible photocatalytic activity. Materials Letters, 2016, 163: 130-133.

[56] Wang S C, Cai J S, Mao J J, et al. Defective black Ti^{3+} self-doped TiO_2 and reduced graphene oxide composite nanoparticles for boosting visible-light driven photocatalytic and photoelectrochemical activity. Applied Surface Science, 2019, 467: 45-55.

[57] Jiang X D, Zhang Y P, Jiang J, et al. Characterization of oxygen vacancy associates within hydrogenated TiO_2: A positron annihilation study. The Journal of Physical Chemistry C, 2012, 116(42): 22619-22624.

[58] Pradenas M, Yanez J, Ranganathan S, et al. Multivariate approach to hydrogenated TiO_2 photocatalytic activity under visible light. Water Environment Research, 2019, 91(2): 157-164.

[59] An H R, Park S Y, Kim H, et al. Advanced nanoporous TiO_2 photocatalysts by hydrogen plasma for efficient solar-light photocatalytic application. Scientific Reports, 2016, 6(1): 29683.

[60] Wang X T, Li Y M, Liu X, et al. Preparation of Ti^{3+} self-doped TiO_2 nanoparticles and their visible light photocatalytic activity. Chinese Journal of Catalysis, 2015, 36(3): 389-399.

[61] Han L J, Su B T, Liu G, et al. A facile microwaving method to turn titanium oxide into highly active Ti^{3+} self-doped structure. Journal of Nanoscience and Nanotechnology, 2016, 16(9): 9826-9831.

[62] Li G L, Li J, Li G, et al. N and Ti^{3+} co-doped 3D anatase TiO_2 superstructures composed of ultrathin nanosheets with enhanced visible light photocatalytic activity. Journal of Materials Chemistry A, 2015, 3(44): 22073-22080.

[63] Zhang H, Xing Z P, Zhang Y, et al. Ni^{2+} and Ti^{3+} co-doped porous black anatase TiO_2 with unprecedented-high visible-light-driven photocatalytic degradation performance. RSC Advances, 2015, 5(129): 107150-107157.

[64] Du J M, Wang H M, Chen H J, et al. Synthesis and enhanced photocatalytic activity of black porous Zr-doped TiO_2 monoliths. Nano, 2016, 11(6): 1650068.

[65] Nawaz R, Kait C F, Chia H Y, et al. Glycerol-mediated facile synthesis of colored titania nanoparticles for visible light photodegradation of phenolic compounds. Nanomaterials, 2019, 9(11): 1586.

[66] Han K, Zhang X, Wang H F, et al. A facile microwaving method to turn titanium oxide into highly active Ti^{3+} self-doped structure. Journal of Nanoscience and Nanotechnology, 2016, 16(9): 9826-9831.

[67] Zhou G, Meng H Y, Cao Y, et al. Surface plasmon resonance-enhanced solar-driven photocatalytic performance from Ag nanoparticles-decorated Ti^{3+} self-doped porous black TiO_2 pillars. Journal of Industrial and Engineering Chemistry, 2018, 64: 188-193.

[68] Qiao P Z, Sun B J, Li H Z, et al. Surface plasmon resonance-enhanced visible-NIR-driven photocatalytic and photothermal catalytic performance by Ag/mesoporous black TiO_2 nanotube heterojunctions. Chemistry—An Asian Journal, 2019, 14(1): 177-186.

[69] Bazzanella N, Bajpai O P, Fendrich M, et al. Ciprofloxacin degradation with a defective TiO_{2-x} nanomaterial under sunlight. MRS Communications, 2023, 13(6): 1252-1259.

[70] Feng X Y, Wang P F, Hou J, et al. Oxygen vacancies and phosphorus codoped black titania coated carbon nanotube composite photocatalyst with efficient photocatalytic performance for the degradation of acetaminophen under visible light irradiation. Chemical Engineering Journal, 2018, 352: 947-956.

[71] Wu S Q, Li X Y, Tian Y Q, et al. Excellent photocatalytic degradation of tetracycline over black anatase-TiO_2 under visible light. Chemical Engineering Journal, 2021, 406: 126747.

[72] Ren L P, Zhou W, Sun B J, et al. Defects-engineering of magnetic γ-Fe_2O_3 ultrathin nanosheets/mesoporous black TiO_2 hollow sphere heterojunctions for efficient charge separation and the solar-driven photocatalytic mechanism of tetracycline degradation. Applied Catalysis B: Environmental, 2019, 240: 319-328.

[73] He J H, Ye J, Zhang Y, et al. Synergistic RGO/black TiO_2/2D-ZIF-8 ternary heterogeneous composite with highly efficient photocatalytic activity. ChemistrySelect, 2020, 5(12): 3746-3755.

[74] Cao Y, Xing Z P, Hu M Q, et al. Mesoporous black N-TiO_2-hollow spheres as efficient visible-light-driven photocatalysts. Journal of Catalysis, 2017, 356: 246-254.

[75] Yan Z Y, Huang W X, Jiang X R, et al. Hollow structured black TiO_2 with thickness-controllable microporous shells for enhanced visible-light-driven photocatalysis. Microporous and Mesoporous Materials, 2021, 323: 111228.

[76] Li G S, Lian Z C, Li X, et al. Ionothermal synthesis of black Ti^{3+}-doped single-crystal TiO_2 as an active photocatalyst for pollutant degradation and H_2 generation. Journal of Materials Chemistry A, 2015, 3(7): 3748-3756.